Volcano-induced regime shifts in millennial tree-ring chronologies from northeastern North America

Fabio Gennaretti[a,1], Dominique Arseneault[a], Antoine Nicault[b], Luc Perreault[c], and Yves Bégin[d]

[a]Département de Biologie, Chimie et Géographie, Centre d'Études Nordiques, Université du Québec à Rimouski, Rimouski, QC, Canada G5L 3A1; [b]Aix-Marseille Université, Fédération de recherche (CNRS-3098) Ecosystèmes Continentaux et Risques Environnementaux, F-13545 Aix-en-Provence, France; [c]Expertise Mécanique, Métallurgie et Hydro-Éolien, Institut de Recherche d'Hydro-Québec, Varennes, QC, Canada J3X 1S1; and [d]Centre Eau Terre Environnement, Institut National de la Recherche Scientifique, Québec, QC, Canada G1K 9A9

Edited by Ellen S. Mosley-Thompson, The Ohio State University, Columbus, OH, and approved May 29, 2014 (received for review January 21, 2014)

Dated records of ice-cap growth from Arctic Canada recently suggested that a succession of strong volcanic eruptions forced an abrupt onset of the Little Ice Age between A.D. 1275 and 1300 [Miller GH, et al. (2012) *Geophys Res Lett* 39(2):L02708, 10.1029/2011GL050168]. Although this idea is supported by simulation experiments with general circulation models, additional support from field data are limited. In particular, the Northern Hemisphere network of temperature-sensitive millennial tree-ring chronologies, which principally comprises Eurasian sites, suggests that the strongest eruptions only caused cooling episodes lasting less than about 10 y. Here we present a new network of millennial tree-ring chronologies from the taiga of northeastern North America, which fills a wide gap in the network of the Northern Hemisphere's chronologies suitable for temperature reconstructions and supports the hypothesis that volcanoes triggered both the onset and the coldest episode of the Little Ice Age. Following the well-expressed Medieval Climate Anomaly (approximately A.D. 910–1257), which comprised the warmest decades of the last millennium, our tree-ring-based temperature reconstruction displays an abrupt regime shift toward lower average summer temperatures precisely coinciding with a series of 13th century eruptions centered around the 1257 Samalas event and closely preceding ice-cap expansion in Arctic Canada. Furthermore, the successive 1809 (unknown volcano) and 1815 (Tambora) eruptions triggered a subsequent shift to the coldest 40-y period of the last 1100 y. These results confirm that series of large eruptions may cause region-specific regime shifts in the climate system and that the climate of northeastern North America is especially sensitive to volcanic forcing.

black spruce | dendroclimatology | lake subfossil trees | *Picea mariana* | temperature regime shifts

Tree-ring chronologies are the type of proxy record most used to develop climate reconstructions covering the last millennium (1). These chronologies have been integrated into large-scale networks, often with additional proxies, to document the amplitude, duration, and forcing mechanisms of the Medieval Climate Anomaly, the Little Ice Age, and the recent warming trend. However, the spatial coverage of long tree-ring records must be improved to allow a better understanding of regional variations in past climate (1, 2). For example, in eastern North America, millennial climate reconstructions have been constructed from tree species and sites sensitive to drought and precipitation (3), whereas temperatures were inferred solely from low-resolution proxies, such as pollen data (4, 5). Furthermore, only tree-ring-based climate reconstructions shorter than a millennium or using chronologies poorly replicated before A.D. 1500 have been published for the entire North American boreal forest (6, 7), whereas several millennial, highly replicated, temperature-sensitive tree-ring records have been developed across the Eurasian boreal zone. This lack of data is an important issue that causes the poor representation of North America in long-term, large-scale temperature reconstructions (1, 4).

The feasibility of reconstructing volcanic forcing from tree-ring data has been debated, especially in regards to large and successive eruptions. Two of the largest eruptions of the last millennium, the A.D. 1257 Samalas and A.D. 1815 Tambora events, were both closely followed and preceded by additional large eruptions in 1227, 1275, 1284, 1809, and 1835 (8–11). Whereas general circulation model experiments suggest that the impacts of large and successive eruptions might have influenced climate systems for periods ranging from 20 y to several decades, or even centuries (12–16), Northern Hemisphere tree-ring-based temperature reconstructions only display negative temperature anomalies lasting between 2 and 10 y (17–20). Region-specific responses of the climate system to volcanic forcing may in part explain this discrepancy (17). For example, large and successive eruptions may have had stronger impacts on summer temperatures in northeastern North America (hereafter NENA) than elsewhere. An extensive Northern Hemisphere network of tree-ring density chronologies supports this idea, showing that the coldest 1816 temperature anomalies occurred over the Quebec-Labrador Peninsula (21), where they may have persisted for several decades (7). The idea is also supported by the abrupt acceleration of ice-cap growth in the Eastern Canadian Arctic during A.D. 1275–1300, at the onset of the Little Ice Age, as a consequence of a series of eruptions (22). However, the lack of millennial, well-replicated, and temperature-sensitive tree-ring chronologies in the NENA sector precludes the examination of the volcano–temperature relationship in a long-term context with an annual resolution.

Significance

The cooling effect on the Earth's climate system of sulfate aerosols injected into the stratosphere by large volcanic eruptions remains a topic of debate. While some simulation and field data show that these effects are short-term (less than about 10 years), other evidence suggests that large and successive eruptions can lead to the onset of cooling episodes that can persist over several decades when sustained by consequent sea ice/ocean feedbacks. Here, we present a new network of millennial tree-ring chronologies suitable for temperature reconstructions from northeastern North America where no similar records are available, and we show that during the last millennium, persistent shifts toward lower average temperatures in this region coincide with series of large eruptions.

Author contributions: F.G., D.A., A.N., L.P., and Y.B. designed research; F.G., D.A., A.N., and L.P. performed research; F.G. analyzed data; and F.G. and D.A. wrote the paper.

The authors declare no conflict of interest.

This article is a PNAS Direct Submission.

Data deposition: All tree-ring and temperature data can be found in Dataset S1 and have been deposited to the World Data Center for Paleoclimatology, http://www.ncdc.noaa.gov/paleo/paleo.html (study ID noaa-recon-16558).

[1]To whom correspondence should be addressed. E-mail: Fabio.Gennaretti@uqar.ca.

This article contains supporting information online at www.pnas.org/lookup/suppl/doi:10.1073/pnas.1324220111/-/DCSupplemental.

In this study, we have built a network of six highly replicated millennial tree-ring chronologies from large stocks of black spruce [*Picea mariana* (Mill.) B.S.P.] subfossil trees preserved in lakes of the NENA taiga from which we developed a millennial reconstruction (A.D. 910–2011) of regional July–August temperatures. For this purpose, we selected homogeneous sites with infrequent and well-documented ecological disturbances (23), and sampled homogeneous subfossil and living samples to maximize the robustness of our reconstruction. We then used a Bayesian mixture of probability distributions with dependence (also referred to as hidden Markov models or Markov switching models; see refs. 24 and 25) to detect possible regime shifts in summer temperatures triggered by series of large eruptions and to provide new insights concerning the climate history of NENA during the last 1,100 y.

Results and Discussion

Our summer temperature reconstruction for Eastern Canada (hereafter STREC) closely reproduces the warming trend of July–August temperatures over the study area during the last century (Fig. 1*A*), even when the region experienced one of the strongest increases in summer temperatures worldwide according to the gridded temperature dataset Climate Research Unit (CRU) TS3.20 (26). The correlation between STREC and the gridded July–August temperature data (1905–2011; CRU TS3.20) is highly significant (0.61, $P < 0.001$), even when the instrumental period is split into two subsets (1905–1957 and 1958–2011; Fig. 1*A*). The skill of the reconstruction in reproducing temperature data is indicated by the positive values of the reduction-of-error statistics computed with different calibration periods and on unsmoothed and smoothed datasets (Table S1). Cross-calibration verification confirms that STREC is robust and better predicts low frequencies than high frequencies (Table S1). In our study, the ring-width series of the subfossil and living tree samples were homogenized to remove the bias caused by varying sampling heights (see *Methods*) and avoid divergence between temperatures and standardized tree growth (Figs. S1 and S2). Spatial

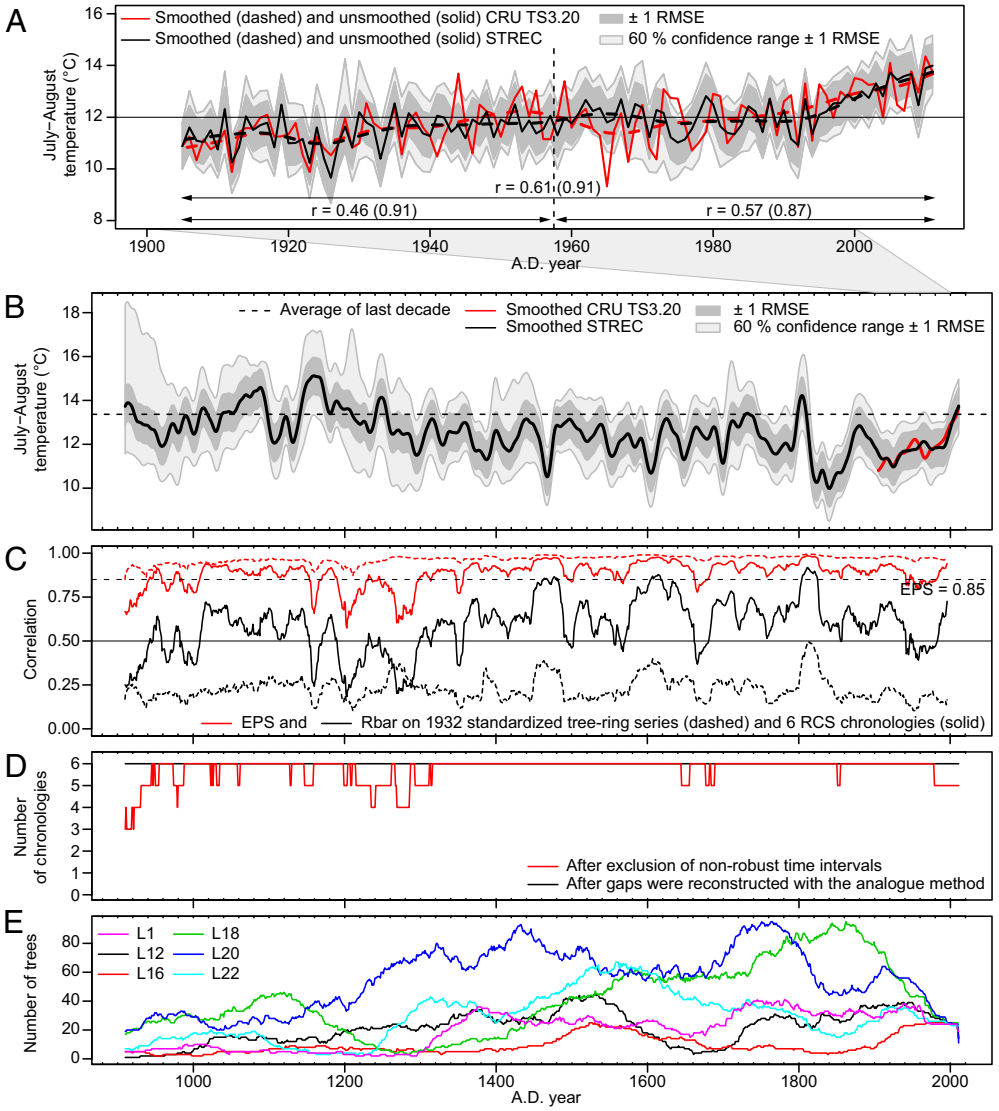

Fig. 1. STREC reconstructed values and robustness. Observed (15 cells of the CRU TS3.20 dataset covering our sampling sites) and reconstructed (STREC) July–August temperatures in the taiga of Eastern Canada during the last century (*A*) and the last 1,100 y (*B*). Smoothed values are 20-y splines. In *A*, correlations between brackets refer to smoothed values. Expressed Population Signal (EPS) and Rbar statistics computed over 31-y moving windows are also shown (*C*), as well as replication among (*D*) and within (*E*) chronologies.

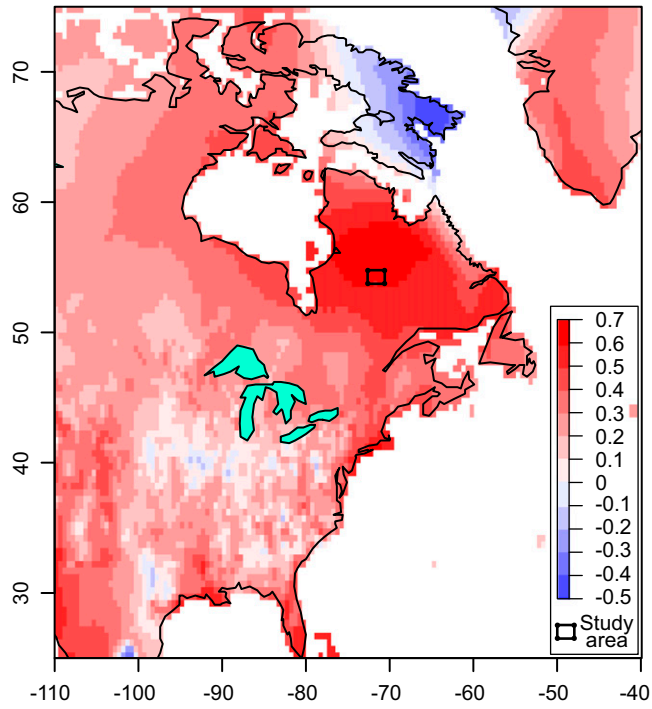

Fig. 2. STREC spatial domain. Spatial variation of the correlation between observed (CRU TS3.20) and reconstructed (STREC) July–August temperatures over the 1905–2011 period.

correlations show that STREC is mostly valid over the central Quebec-Labrador Peninsula within the NENA sector (Fig. 2).

Volcanism has been the primary factor forcing changes in summer temperatures on the decadal time scale in Eastern Canada during the last millennium. Numerous cooling episodes in STREC are synchronous with episodes already reported in hemispheric temperature reconstructions and simulations in response to strong volcanic eruptions (Fig. S3). The agreement between peaks in the global stratospheric volcanic sulfate aerosol injections (9) and cold anomalies inferred by STREC is also striking (Fig. 3*A*). A Superimposed Epoch Analysis (*SI Methods*) demonstrates that the 10 strongest volcanic eruptions of the last millennium produced highly significant cooling episodes in Eastern Canada lasting for about two decades, while less intense volcanic eruptions had a shorter influence (Fig. 4). The 20 postevent summers were significantly colder than the preceding ones for 8 out of the 10 largest eruptions ($P < 0.1$; Table S2). For example, temperature anomalies ranged from −1.3 °C to −3.0 °C in response to the three strongest tropical eruptions of the last millennium (A.D. 1257, 1452/1453, and 1815). With about two cooling episodes per century lasting for 10–20 y with a consequent reduction in tree growth, the volcanic signature in the NENA taiga is comparable to the epidemic signal of the eastern spruce budworm (*Choristoneura fumiferana*), which is the most destructive insect in the commercial forest of Eastern Canada south of our study area (27). Therefore, volcanic forcing during the last millennium has clearly impacted net primary production and the carbon balance in the NENA forests, at least over the Quebec-Labrador taiga.

Volcanism also strongly influenced century-scale temperature variability in NENA, as shown by our Bayesian analysis of regime shifts in STREC (*SI Methods*). Two of the strongest eruptions of the last 1,100 y, the A.D. 1257 Samalas and A.D. 1815 Tambora events, which were followed and preceded by other eruptions, coincide exactly with the two most persistent regime shifts detected in STREC. According to the Schwarz criterion (28), STREC is best modeled with a four-state normal Bayesian hidden Markov model, with the two warmer and the two colder regimes largely dominating the A.D. 910–1257 and A.D. 1816–2011 time periods, respectively (Fig. 3*B* and Fig. S4). Other studies based on tree-ring data have already reported temperature reductions post-A.D. 1257 and post-A.D. 1815 in other regions of the world (see, for example, refs. 29 and 30), but with smaller amplitude and temporal extent than STREC. Indeed, the strong overall cooling trend obtained by fitting a linear regression model to STREC (−1.60 ± 0.11 °C per 1,000 y; estimate ± SE; $P < 0.001$) can be mostly attributed to the A.D. 1257 and A.D. 1815 shifts. Some proxy-based evidence has also shown that a long-term cooling trend due to orbital changes has characterized the climate of the last 2,000 y in many regions of the world (4, 31, 32), including NENA (33). However, this cooling trend has been estimated at about −0.3 °C to −0.5 °C per 1,000 y (4, 32, 33) and is much weaker than the one of STREC. These facts, in addition to the absence of any negative trends in STREC over the A.D. 1257–1815 time period (Fig. S5), highlight the importance of volcanic-induced temperature regime shifts in NENA. Along with volcanism and orbital forcing, additional factors may have contributed to the strong negative trend of STREC and the associated transition from warm to cold regimes (Fig. 3*B* and Figs. S4 and S5), including solar forcing (19), and the specific regional domain of STREC. Because STREC is based on several sites and because of our data management approach (see *Methods*), the A.D. 1257 and A.D. 1815 shifts do not seem to be influenced by local nonclimatic disturbances affecting our chronologies (Fig. S6).

A well-expressed Medieval Climate Anomaly (A.D. 910–1257) occurred in NENA before the A.D. 1257 Samalas event. The warmest decades reconstructed by STREC occurred between A.D. 1141 and 1170 (positive anomalies ranging from 0.89 °C to 1.80 °C with respect to the last decade) and between A.D. 1061 and 1095 (0.87–1.19 °C; Table S3). The confidence intervals of STREC for these two periods were almost all higher than the mean temperatures of the last decade (Fig. 1*B*). The amplitude and timing of the Medieval Climate Anomaly reconstructed by STREC also resemble the results of a pollen-based temperature reconstruction for the North American forest tundra (5), and closely correspond to a period of ice-cap melting in the Eastern Canadian Arctic (22) (Fig. 3*A*). Collectively, these complementary data sources demonstrate that a major and prolonged climatic shift occurred over the NENA sector after a series of 13th century volcanic eruptions centered around the A.D. 1257 Samalas event. This shift marked the end of the Medieval Climate Anomaly and the beginning of the Little Ice Age in this sector.

Similarly, the series of eruptions centered around the A.D. 1815 Tambora event shifted summer temperatures to the coldest 40-y period of the last 1,100 y in NENA. The A.D. 1815–1857 episode was extremely cold in Eastern Canada, with decadal anomalies reconstructed by STREC ranging from −2.76 °C to −3.58 °C relative to the last decade (Table S3). Low solar activity during this period, that started during the Dalton Minimum, could have concurred to cause the cooling episode (34). However, the regime shift observed in STREC coincides with the A.D. 1815 Tambora eruption (Fig. 3*B* and Fig. S4). The same climate shift has already been observed in a 263-y tree-ring-based summer temperature reconstruction whose sampling sites are 400 km eastward from our study sites (7), whereas a pollen-based temperature reconstruction suggests that this period was the coldest of the last 2,000 y in the North American boreal forest and forest–tundra (5). This climate shift was probably limited to the NENA sector as STREC diverges from the ensemble of Northern Hemisphere reconstructions and simulations after A.D. 1816 (Fig. S3 *C* and *D*).

Although the last century reconstructed by STREC was warmer than the early 19th century, it was colder than the

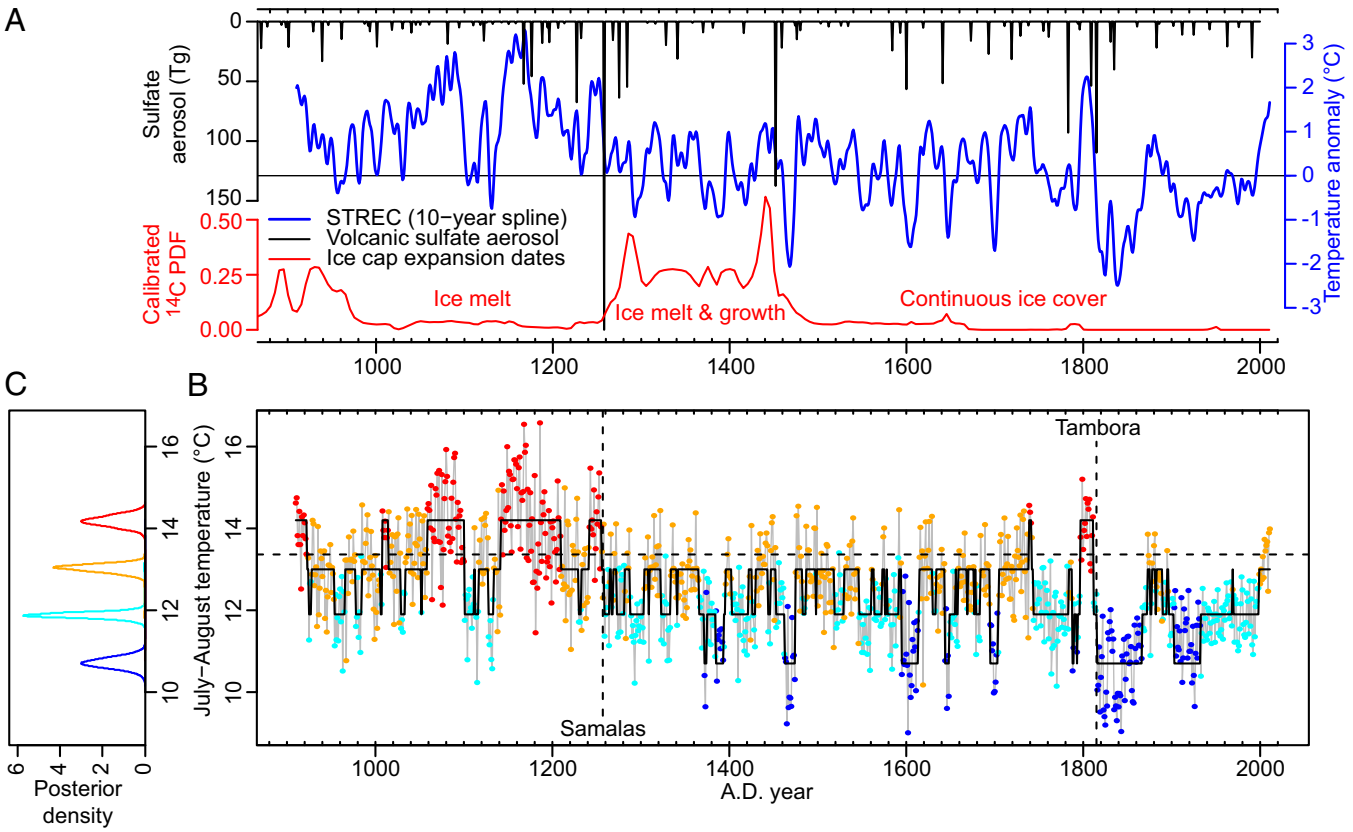

Fig. 3. Volcano-induced regime shifts in STREC. Comparison (*A*) between STREC, a reconstruction of global stratospheric volcanic sulfate aerosol injections (9), and a reconstruction of ice-cap expansion dates from Arctic Canada (22). Detected regime shifts in STREC based on a four-component Bayesian hidden Markov model with normal probability distributions (*SI Methods*) are also shown (*B*), as well as the posterior probability density functions of the mean temperature of each regime (*C*). In *B*, each reconstructed value is assigned to the most likely regime (color dots) and the mean temperature of the last decade is shown (horizontal dashed lines), as well as the dates of the A.D. 1257 Samalas and A.D. 1815 Tambora eruptions (vertical dashed lines).

Medieval Climate Anomaly (the difference between the average summer temperature of the 12th century and of the last 100 y is 1.66 °C, $P < 0.001$, according to the one-tailed Wilcoxon rank–sum test). In fact, STREC shows that the NENA sector experienced relatively cold conditions until late into the 20th century. This persistence of cold conditions over NENA is also suggested by the strong warming trend of the last 100 y denoting a colder starting point (Fig. 1 *A* and *B*), as well as by permafrost growth during the mid-20th century on the southern shore of Hudson Strait (35) and by the lack of postfire forest recovery over the last 900 y at the northern Quebec treeline in contrast to what occurred during the Medieval Climate Anomaly (36, 37). The warming trend in our study area has accelerated over the last 30 y (+0.7 °C per decade according to the dataset CRU TS3.20). If this trend continues, then summer temperatures will be similar to the maximum of the last 750 y during the next decade and to the maximum of the last 1,100 y during the following one (based on STREC and the data of Table S3).

Several hypotheses have been suggested to explain why post-eruption temperature anomalies reconstructed from tree-ring data generally express higher values than expected, including regional variations in response to volcanic events, autocorrelation in ring-width series (17, 18), failure of growth rings to form during volcano-induced cold summers (20), and increased tree growth caused by volcano-induced diffuse radiation (38). In this study, we observed a strong response of ring-width data to volcanic activity, with the amplitudes and duration of negative anomalies (including persistent regime shifts) similar to model predictions. Diagnostic light rings are frequent in black spruce trees of our study area (39), thus allowing for a rigorous control of ring dating and for identifying the occurrence of missing rings. In addition, although autocorrelation in ring-width chronologies of black spruce is high (Table 1), the results of a simple model show that its effects on the amplitude and duration of reconstructed negative temperature anomalies after volcanic events are low (Fig. S7). Instead, our results suggest that the climatic impacts of eruptions vary among regions of the Northern Hemisphere and that the NENA sector is especially sensitive to these impacts compared with Eurasia, where the majority of temperature-sensitive tree-ring chronologies have been previously developed. This idea is also supported by recent simulation experiments (12–16, 22), which show that large and successive eruptions may trigger cold episodes whose duration may be sustained by complex and variable sea–ice–ocean feedbacks in the North Atlantic and that the resultant northward heat transport would tend to be more severely attenuated in the NENA than in the Eurasian sectors.

Methods

Our sampling area is situated in the Eastern Canadian taiga between latitudes 53.8°N and 54.6°N and longitudes 70.2°W and 72.5°W (Table 1). According to the gridded temperature dataset CRU TS3.20 (26), this region has experienced one of the fastest temperature increases on Earth during the last century. The mean July–August temperature, which is the object of our reconstruction, has increased by an average of 0.68 ± 0.15 °C and 0.19 ± 0.02 °C (estimate ± SE) each 10 y during the last 30 and the last 110 y, respectively.

To implement our network of tree-ring chronologies, 1782 black spruce [*Picea mariana* (Mill.) B.S.P.] subfossil trees were sampled from six lakes of the study area and cross-dated to the calendar year. Particular care was taken in selecting and replicating sites and trees to construct a dataset

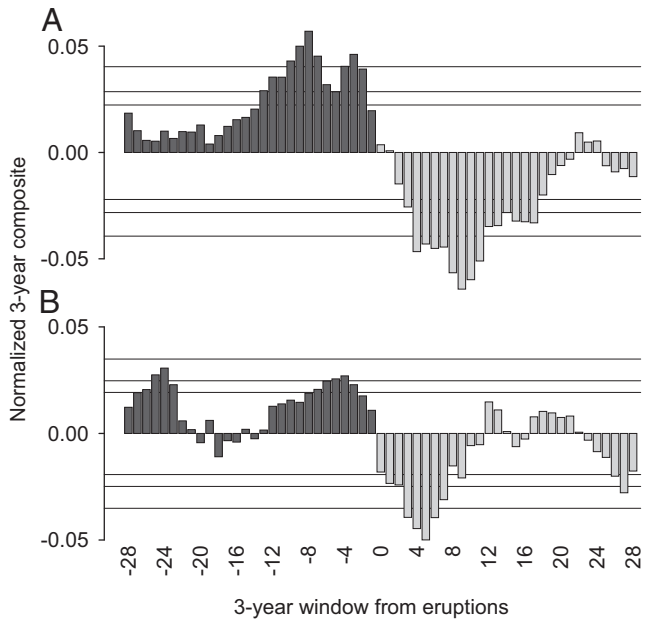

Fig. 4. STREC responses to volcanic eruptions. Dimensionless normalized 3-y composites, which are the result of the Superimposed Epoch Analysis showing summer temperature responses in Eastern Canada to the 10 strongest (*A*) and the 10 next strongest (*B*) volcanic eruptions of the last millennium deduced by ref. 9 (see *SI Methods*). Each 3-y composite is labeled with the year nearest to the eruption year (e.g., 0 stands for the 3-y composite composed of years 0, 1, and 2 from eruption). Confidence ranges (90%, 95%, 99%) are indicated by horizontal lines. Black and gray columns mark preeruption and posteruption composites, respectively.

suitable for Regional Curve Standardization (RCS). The RCS method preserves long-term climate trends in tree-ring chronologies built with short-lived species, but requires high replication of trees belonging to a homogeneous population not disturbed by external factors (40). The selected sites were all characterized by an old-growth riparian forest on the side of the lake protected from dominant winds, an abrupt forest–lake transition, large stocks of subfossil trees in the littoral zone, and a well-documented low fire recurrence (23, 41). This allowed the development of an exceptional network of climate-sensitive tree-ring data comprising six local chronologies in the same region (one per lake), each including from 75 to 586 subfossil trees and spanning from 1,238 to 1,440 y (Table 1). The living trees extending the chronologies to the present day (25 trees per site) were sampled at the same sites as the subfossil samples, and issues related to tree selection and sampling height were also considered (see below).

To produce the six local chronologies (Fig. S3), two radii were measured at a precision of 1/100 mm and then averaged for each tree. A spline with a 50% frequency cutoff and a time-varying response [starting at 10 y and increasing by one each year (42)] was used as a smoothing algorithm to generate the local growth curves needed for RCS standardization. All specimens had well-preserved piths, and pith offset could easily be accounted for in the chronology development.

To guarantee homogeneity between subfossil and living samples, 25 living trees at each site were selected from among those growing near the lakeshore, as they would be the most likely to have generated subfossil stems (32). Furthermore, we considered that the growth trends of subfossil and living samples can diverge depending on the sampling height of the living trees (43), thus generating biases in the RCS chronologies. To reduce these biases, we sampled all living trees at four meters above the soil surface (i.e., the sampling height that minimized the differences between the growth trends of living and subfossil trees) and we corrected all ring-width series before standardization by subtracting the difference between the local growth curves of the living and subfossil trees (see Figs. S1 and S2).

All of the nonrobust time intervals of the local RCS chronologies were discarded, with the resulting gaps being reconstructed using the analog method (44). Most of these intervals were asynchronous among the lakes and were caused by wildfires that temporarily reduced the input of tree remains into the littoral zone (23, 41). We identified the nonrobust time intervals using the Rbar statistic (mean correlation between pairs of individual series) over 31-y moving windows and discarded all intervals with negative or noncomputable Rbar values due to low replication. At lake L16, the 1978–2011 period was also discarded, as the construction of a road raised the lake water level and disturbed the riparian trees. Over the 1,102 y retained for STREC (see below), we discarded 114, 70, 52, 19, 0, and 31 y for lakes L1, L12, L16, L18, L20, and L22, respectively. The analog method used to reconstruct these gaps is commonly used in paleoclimatology to estimate missing values in proxy-climate matrices. For years where missing values are present, the procedure identifies the most similar years in the calibration period, i.e., all other years without missing values, which are then weighted according to their similarity and used to reconstruct the gaps (44). The measure of similarity is based on the Euclidian distance.

We used the CRU TS3.20 climate dataset (26) to calibrate our reconstruction. The first four years (1901–1904) were excluded because of a poor fit with the tree-ring indexes due to the lack of operating weather stations at the beginning of the last century near the study area. The climate reconstruction method was based on a linear scaling procedure. Each local RCS chronology was rescaled so that its mean and SD matched those of the July–August mean temperature in the calibration period (1905–2011). The final STREC was then obtained by computing the median of the six local reconstructions. This approach attenuated the influence of local nonclimatic disturbances, as the median of the six reconstructions is not sensitive to outliers. It also obtained better cross-calibration verification results (1905–1957 vs. 1958–2011) than a reconstruction based on a partial least squares regression, especially when considering low frequencies (i.e., smoothed datasets; Table S1). Only reconstructed values subsequent to A.D. 910 were retained to limit the analyzed period to the statistically reliable interval (overall replication >53 individual series and Expressed Population Signal >0.85; Fig. 1 *C* and *E*). Due to the fast temperature increase in the study area during the 20th century, the reconstructed values in the calibration encompassed a range of 4.3 °C (from 9.6 °C to 14.0 °C), and 86% of the total STREC reconstructed values are inside this range.

We generated realistic time-varying confidence intervals considering two kinds of errors (Fig. 1 *A* and *B*). The first one depends on the nonperfect fit between observed and reconstructed values over the verification periods and was computed as the mean root-mean-square error between the two datasets. The second one is due to the variation over time of the strength of the common climate signal for each of the six local chronologies and was computed each year as the interval among the four central reconstructed values from the six chronologies. The consideration of this error produces a time-varying 60% confidence interval.

Table 1. Sampling sites and tree-ring chronologies used for STREC

Site	Latitude, degrees	Longitude, degrees	Number of trees, subfossil/living	Length, A.D.	MSL, years ± SD	Mean ring width, 1/100 mm ± SD	Mean correlation, mean ± SD	Lag1 AC	AR order
L1	+53.86	−72.41	190/25	642–2011	106 ± 32	39 ± 24	0.43 ± 0.25	0.84	4
L12	+54.46	−70.39	220/25	572–2011	101 ± 32	42 ± 23	0.45 ± 0.23	0.78	9
L16	+54.10	−71.63	75/25	774–2011	112 ± 36	37 ± 20	0.46 ± 0.25	0.75	10
L18	+54.25	−72.38	419/25	596–2011	105 ± 38	38 ± 26	0.40 ± 0.27	0.76	4
L20	+54.56	−71.24	586/25	653–2011	102 ± 36	40 ± 24	0.41 ± 0.23	0.72	9
L22	+54.15	−70.29	292/25	650–2011	104 ± 38	39 ± 25	0.42 ± 0.25	0.73	6

Lag1 AC and AR order are computed over the time period retained for STREC (A.D. 910–2011). AR order, the order selected by the Akaike Information Criterion of the autoregressive model fitted to the RCS chronology; Lag1 AC, lag 1 autocorrelation of the RCS chronology; mean correlation, average correlation between standardized individual series and their respective local RCS chronology; MSL, mean segment length.

The volcanic signature in STREC was analyzed using Superimposed Epoch Analysis (SEA) and Bayesian hidden Markov models. We used SEA to test the agreement between the strongest volcanic eruptions of the last millennium and corresponding cooling episodes in STREC. Our SEA was performed in the R environment as described in *SI Methods*. We used Bayesian hidden Markov models to identify sudden changes in the STREC time series. Such models provide an explicit mechanism to represent transitions between different states and allowed the data to be classified into distinct regimes. The Schwarz criterion is used to identify the number of states and the probability distribution that best fits the data. This approach is briefly described in *SI Methods*.

All tree-ring and temperature data are included in the Dataset S1 and will also be available from the World Data Center for Paleoclimatology (http://www.ncdc.noaa.gov/paleo/paleo.html).

ACKNOWLEDGMENTS. The authors wish to thank Julia Autin, Yves Bouthillier, Pierre-Paul Dion, Sébastien Dupuis, Benjamin Dy, and Joëlle Marion for field and laboratory assistance; Aurore Catalan for technical assistance; and Joel Guiot for its comments on the paper. This research is a contribution from the ARCHIVES project (http://archives.ete.inrs.ca/) and was financially supported by the Natural Sciences and Engineering Research Council of Canada, Hydro-Quebec, Ouranos, ArcticNet, the EnviroNorth training program, and the Centre for Northern Studies.

1. Jansen E, et al. (2007) Palaeoclimate. *Climate Change 2007: The Physical Science Basis. Contribution of Working Group I to the Fourth Assessment Report of the Intergovernmental Panel on Climate Change*, eds Solomon S, et al. (Cambridge Univ Press, Cambridge, UK), pp 433–497.
2. Jones PD, et al. (2009) High-resolution palaeoclimatology of the last millennium: A review of current status and future prospects. *Holocene* 19(1):3–49.
3. Stahle DW, et al. (2012) Tree-ring analysis of ancient baldcypress trees and subfossil wood. *Quat Sci Rev* 34:1–15.
4. PAGES 2k Consortium (2013) Continental-scale temperature variability during the past two millennia. *Nat Geosci* 6:339–346.
5. Viau AE, Ladd M, Gajewski K (2012) The climate of North America during the past 2000 years reconstructed from pollen data. *Global Planet Change* 84-85:75–83.
6. D'Arrigo R, Wilson R, Jacoby G (2006) On the long-term context for late twentieth century warming. *J Geophys Res* 111(D3):D03103, 10.1029/2005JD006352.
7. Jacoby GC, Ivanciu IS, Ulan LD (1988) A 263-year record of summer temperature for northern Quebec reconstructed from tree-ring data and evidence of a major climatic shift in the early 1800's. *Palaeogeogr Palaeoclimatol Palaeoecol* 64(1-2):69–78.
8. Lavigne F, et al. (2013) Source of the great A.D. 1257 mystery eruption unveiled, Samalas volcano, Rinjani Volcanic Complex, Indonesia. *Proc Natl Acad Sci USA* 110(42):16742–16747.
9. Gao C, Robock A, Ammann C (2008) Volcanic forcing of climate over the past 1500 years: An improved ice core-based index for climate models. *J Geophys Res* 113(23):D23111, 10.1029/2008JD010239.
10. Crowley TJ (2000) Causes of climate change over the past 1000 years. *Science* 289(5477):270–277.
11. Cole-Dai J, et al. (2009) Cold decade (AD 1810–1819) caused by Tambora (1815) and another (1809) stratospheric volcanic eruption. *Geophys Res Lett* 36(22):L22703, 10.1029/2009GL040882.
12. Schleussner CF, Feulner G (2013) A volcanically triggered regime shift in the subpolar North Atlantic Ocean as a possible origin of the Little Ice Age. *Clim Past* 9(3):1321–1330.
13. Zhong Y, et al. (2011) Centennial-scale climate change from decadally-paced explosive volcanism: A coupled sea ice-ocean mechanism. *Clim Dyn* 37(11-12):2373–2387.
14. Zanchettin D, et al. (2012) Bi-decadal variability excited in the coupled ocean–atmosphere system by strong tropical volcanic eruptions. *Clim Dyn* 39(1-2):419–444.
15. Stenchikov G, et al. (2009) Volcanic signals in oceans. *J Geophys Res* 114(D16):D16104, 10.1029/2008JD011673.
16. Otterå OH, Bentsen M, Drange H, Suo L (2010) External forcing as a metronome for Atlantic multidecadal variability. *Nat Geosci* 3(10):688–694.
17. D'Arrigo R, Wilson R, Anchukaitis KJ (2013) Volcanic cooling signal in tree ring temperature records for the past millennium. *J Geophys Res* 118(16):9000–9010.
18. Esper J, et al. (2013) European summer temperature response to annually dated volcanic eruptions over the past nine centuries. *Bull Volcanol* 75(7):1–14.
19. Breitenmoser P, et al. (2012) Solar and volcanic fingerprints in tree-ring chronologies over the past 2000 years. *Palaeogeogr Palaeoclimatol Palaeoecol* 313-314:127–139.
20. Mann ME, Fuentes JD, Rutherford S (2012) Underestimation of volcanic cooling in tree-ring-based reconstructions of hemispheric temperatures. *Nat Geosci* 5(3):202–205.
21. Briffa KR, Jones PD, Schweingruber FH, Osborn TJ (1998) Influence of volcanic eruptions on Northern Hemisphere summer temperature over the past 600 years. *Nature* 393(6684):450–455.
22. Miller GH, et al. (2012) Abrupt onset of the Little Ice Age triggered by volcanism and sustained by sea-ice/ocean feedbacks. *Geophys Res Lett* 39(2):L02708, 10.1029/2011GL050168.
23. Gennaretti F, Arseneault D, Bégin Y (2014) Millennial stocks and fluxes of large woody debris in lakes of the North American taiga. *J Ecol* 102(2):367–380.
24. Évin G, Merleau J, Perreault L (2011) Two-component mixtures of normal, gamma, and Gumbel distributions for hydrological applications. *Water Resour Res* 47(8):W08525, 10.1029/2010WR010266.
25. Perreault L, Garçon R, Gaudet J (2007) Analyse de séquences de variables aléatoires hydrologiques à l'aide de modèles de changement de régime exploitant des variables atmosphériques [Modelling hydrologic time series using regime switching models and measures of atmospheric circulation]. *Houille Blanche* 6:111–123. French.
26. Mitchell TD, Jones PD (2005) An improved method of constructing a database of monthly climate observations and associated high-resolution grids. *Int J Climatol* 25(6):693–712.
27. Boulanger Y, et al. (2012) Dendrochronological reconstruction of spruce budworm (*Choristoneura fumiferana*) outbreaks in southern Quebec for the last 400 years. *Can J Res* 42(7):1264–1276.
28. Schwarz G (1978) Estimating the dimension of a model. *Ann Stat* 6(2):461–464.
29. Naurzbaev MM, Vaganov EA (2000) Variation of early summer and annual temperature in east Taymir and Putoran (Siberia) over the last two millennia inferred from tree rings. *J Geophys Res* 105(D6):7317–7326.
30. Salzer MW, Bunn AG, Graham NE, Hughes MK (2014) Five millennia of paleotemperature from tree-rings in the Great Basin, USA. *Clim Dyn* 42(5-6):1517–1526.
31. Kaufman DS, et al.; Arctic Lakes 2k Project Members (2009) Recent warming reverses long-term arctic cooling. *Science* 325(5945):1236–1239.
32. Esper J, et al. (2012) Orbital forcing of tree-ring data. *Nat Clim Change* 2(12):862–866.
33. Miller GH, Lehman SJ, Refsnider KA, Southon JR, Zhong Y (2013) Unprecedented recent summer warmth in Arctic Canada. *Geophys Res Lett* 40(21):5745–5751.
34. Wagner S, Zorita E (2005) The influence of volcanic, solar and CO_2 forcing on the temperatures in the Dalton Minimum (1790–1830): A model study. *Clim Dyn* 25(2-3):205–218.
35. Kasper JN, Allard M (2001) Late-Holocene climatic changes as detected by the growth and decay of ice wedges on the southern shore of Hudson Strait, northern Québec, Canada. *Holocene* 11(5):563–577.
36. Payette S, Morneau C (1993) Holocene relict woodlands at the Eastern Canadian treeline. *Quat Res* 39(1):84–89.
37. Payette S, Filion L, Delwaide A (2008) Spatially explicit fire-climate history of the boreal forest-tundra (Eastern Canada) over the last 2000 years. *Philos Trans R Soc Lond B Biol Sci* 363(1501):2301–2316.
38. Robock A (2005) Cooling following large volcanic eruptions corrected for the effect of diffuse radiation on tree rings. *Geophys Res Lett* 32(6):L06702, 10.1029/2004GL022116.
39. Filion L, Payette S, Gauthier L, Boutin Y (1986) Light rings in subarctic conifers as a dendrochronological tool. *Quat Res* 26(2):272–279.
40. Esper J, Cook ER, Krusic PJ, Peters K, Schweingruber FH (2003) Tests of the RCS method for preserving low-frequency variability in long tree-ring chronologies. *Tree-Ring Res* 59(2):81–98.
41. Arseneault D, Dy B, Gennaretti F, Autin J, Bégin Y (2013) Developing millennial tree ring chronologies in the fire-prone North American boreal forest. *J Quat Sci* 28(3):283–292.
42. Melvin TM, Briffa KR, Nicolussi K, Grabner M (2007) Time-varying-response smoothing. *Dendrochronologia* 25(1):65–69.
43. Clyde MA, Titus SJ (1987) Radial and longitudinal variation in stem diameter increment of lodgepole pine, white spruce, and black spruce: Species and crown class differences. *Can J Res* 17(10):1223–1227.
44. Guiot J, et al. (2005) Last-millennium summer-temperature variations in western Europe based on proxy data. *Holocene* 15(4):489–500.

Supporting Information

Gennaretti et al. 10.1073/pnas.1324220111

SI Methods

Superimposed Epoch Analysis. The Superimposed Epoch Analysis (SEA) is a statistical method that can be used to verify the presence and the significance of systematic responses in a dataset related to particular events occurring during key dates. We used SEA to test the striking agreement between the occurrence of the major volcanic eruptions of the last millennium and some cooling episodes inferred by STREC (summer temperature reconstruction for Eastern Canada). Our analysis was implemented as proposed by ref. 1, which used SEA to study connections between explosive volcanic eruptions and subsequent El Niño climate episodes. Our SEA was performed in the R environment according to the following steps:

First, two subsets of key volcanic dates from the last millennium were selected using the reconstruction of the global stratospheric volcanic sulfate aerosol injections of ref. 2. The 10 y with the highest sulfate aerosol loadings and the 10 y with loading values just below the preceding ones were considered as key dates corresponding to the 10 strongest and the 10 next strongest volcanic eruptions, respectively.

Second, the key volcanic dates were then used to generate two "eruption matrices" with the number of rows equal to the number of eruptions. In each row, we stacked the 30 STREC reconstructed values before and after each eruption date. In this way, two matrices were created with each composed of 10 rows and 61 columns. The values in the matrices were then normalized to attenuate the influence of large anomalies that could have occurred before or after a particular key volcanic date. To do so, the values in each row were divided by the maximum value of the row and, subsequently, the overall mean of the values in each matrix was subtracted from all values.

Third, dimensionless normalized composites, which represent the mean response of summer temperatures in Eastern Canada to each subset of volcanic eruptions, were obtained by averaging the values of each column for each matrix. To evaluate the significance of the obtained composites, we used a Monte Carlo randomization procedure that reshuffles blocks of two values in each row of an eruption matrix, thus creating 10,000 randomly generated eruption matrices. These matrices can then be used to generate 10,000 sets of composites and, subsequently, a random composite distribution for any specific year from a volcanic eruption (in our case, 61 distributions). We used these distributions to test the significance of the obtained composites at the 90%, 95%, and 99% confidence levels. The Monte Carlo randomization procedure is based on reshuffling blocks of two values rather than individual values because this allows randomly generated eruption matrices to be obtained with first-order autocorrelations similar to the original ones.

Fourth, to smooth out annual variations in the results of the SEA, we generated 3-y mean composites from the obtained composites and random 3-y mean composite distributions from the 10,000 randomly generated sets of composites. The final results are illustrated in Fig. 4 and show that the 10 major volcanic eruptions of the last millennium have produced highly significant cooling episodes in Eastern Canada that lasted for about two decades, while less intense volcanic eruptions had a shorter influence. For this reason, we decided also to test whether the 20 or 10 postevent summers were significantly colder than the preceding ones, for each of the 10 strongest and each of the 10 next strongest volcanic eruptions, respectively. The statistical test used was a one-tailed Wilcoxon rank–sum test (Table S2).

Bayesian Analysis of Regime Shifts. Regime shifts in the STREC time series were analyzed using a mixture of probability distributions to which a persistence structure was added. Such probabilistic models are often called hidden Markov models (HMM). Here, they provided an explicit and formal mechanism to detect shifts in the STREC time series and the length of "warm" and "cold" sequences (i.e., the regimes).

HMM are useful when it is suspected that observations in time exhibit persistence in several regimes with occasional transitions between them. While the observations come from distinct populations, it is not possible to identify exactly when the changes took place. HMM are typically specified through a hierarchical structure. In the first level, the way in which the transitions from one state to another occur is formalized. This is done by assuming that the "hidden" states follow a Markov process. The shifts and the persistence of each regime are governed by state transition probabilities. The second level represents the process that generates the data, given the current regime. For a given year, the data are generated from a statistical distribution whose parameters depend upon the current regime. In this study, two statistical probability distributions have been considered: a normal distribution and a lognormal distribution.

The parameters of the models (means, SDs, transition probabilities) are estimated using a Bayesian approach, as presented in detail in ref. 3. The estimation process involves Monte Carlo Markov Chain simulations, since no explicit algebraic solutions are available for the parameter estimates of such models. More specifically, we used Gibbs sampling.

Twelve configurations were considered to model the STREC time series. Bayesian HMM with one to six regimes and two probability distributions were applied (normal and lognormal). In this paper, we chose to compute the Schwarz information criterion (4) to select the best representation of the STREC time series between the competing models. The Schwarz criterion was calculated for each of the 12 configurations and allowed us to formally identify both the number of regimes and which probability distribution best fits the STREC time series. It is important to mention that this criterion takes into account both the statistical goodness of fit and the number of parameters that have to be estimated to achieve this particular degree of fit by imposing a penalty for increasing the number of parameters. We gave preference to the model that maximized the Schwarz criterion.

The estimation of the twelve HMM and the computation of their respective Schwarz criterion were performed in the MATLAB environment using codes developed by Évin et al. (3). The first step in Bayesian analysis is to set up a full probability model. That is, in addition to modeling the observable quantities (i.e., the STREC data) using a HMM, we must represent the prior degree of belief concerning all of the unknowns (i.e., the parameters of the model: means, SDs, and transition probabilities). Here we considered noninformative prior distributions for each parameter and let the data talk for itself. In our case, the Schwarz criterion reported evidence in favor of a four-state Bayesian HMM with normal distributions. This result, which states that a normal distribution is more suitable than a lognormal distribution for our data, is not surprising. In fact, in most meteorological and climatological studies, temperatures are assumed to be normally distributed.

In the Bayesian framework, all statistical inferences about the unknown parameters are based on the posterior distribution. Just as the prior distribution reflects beliefs about the parameters

of the HMM before experimentation, the posterior distribution reflects the updated beliefs after observing the sample data. Fig. 3*C* represents the posterior distributions of the mean temperature of each regime. These distributions do not superimpose, which indicates significant differences between the average temperatures of the four regimes. Furthermore, Fig. S4 (*Lower*) show the posterior distributions of the transition probability p_{kk} of each regime and indicate a strong persistence with a probability to stay in a given regime k greater than 0.8 for all regimes.

Finally, the posterior probabilities that each observation belongs to a given regime can be evaluated. These are presented in Fig. S4 for each regime. These graphs can be used to locate sudden changes from one regime to another and to identify historical sequences of warm or cold temperatures that may have occurred.

1. Brad Adams J, Mann ME, Ammann CM (2003) Proxy evidence for an El Niño-like response to volcanic forcing. *Nature* 426(6964):274–278.
2. Gao C, Robock A, Ammann C (2008) Volcanic forcing of climate over the past 1500 years: An improved ice core-based index for climate models. *J Geophys Res* 113(23): D23111, 10.1029/2008JD010239.
3. Évin G, Merleau J, Perreault L (2011) Two-component mixtures of normal, gamma, and Gumbel distributions for hydrological applications. *Water Resour Res* 47(8):W08525, 10.1029/2010WR010266.
4. Schwarz G (1978) Estimating the dimension of a model. *Ann Stat* 6(2):461–464.

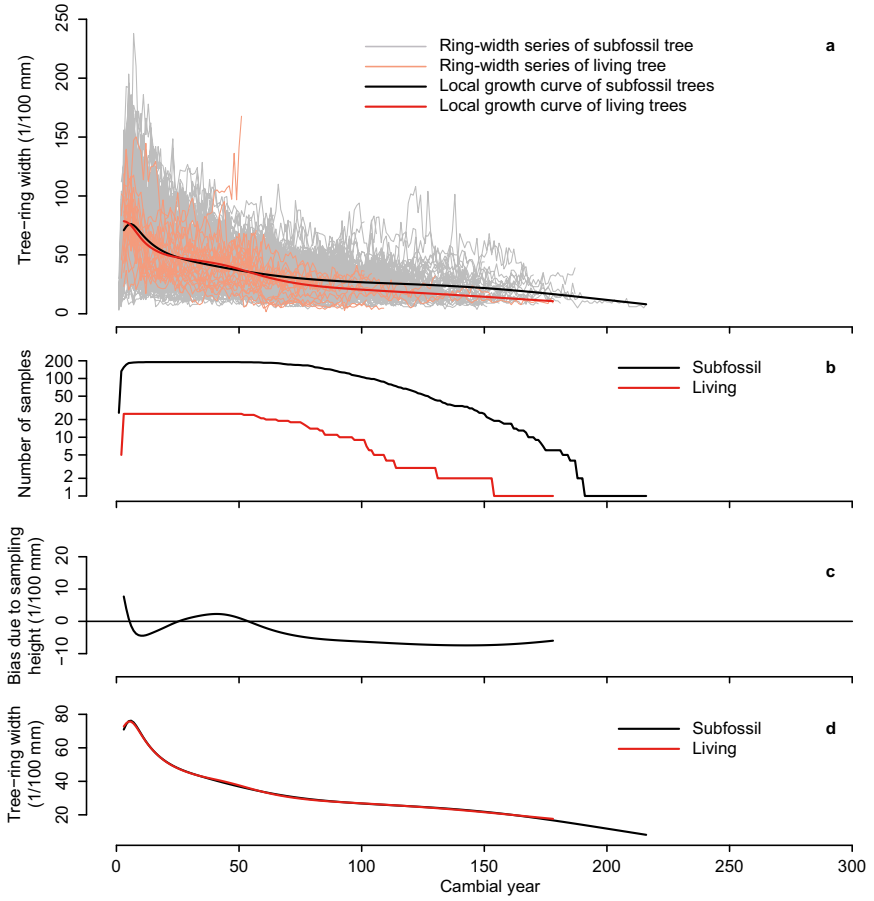

Fig. S1. Local growth curves and homogenization of subfossil and living tree materials. (*A*) The local growth curves of the subfossil and living trees at L1 (site chosen as example), (*B*) their sample replication (logarithmic *y* axis), (*C*) the bias due to sampling height (i.e., difference between local growth curves of living and subfossil trees), and (*D*) the local growth curves after the bias is removed from all ring-width series of living trees.

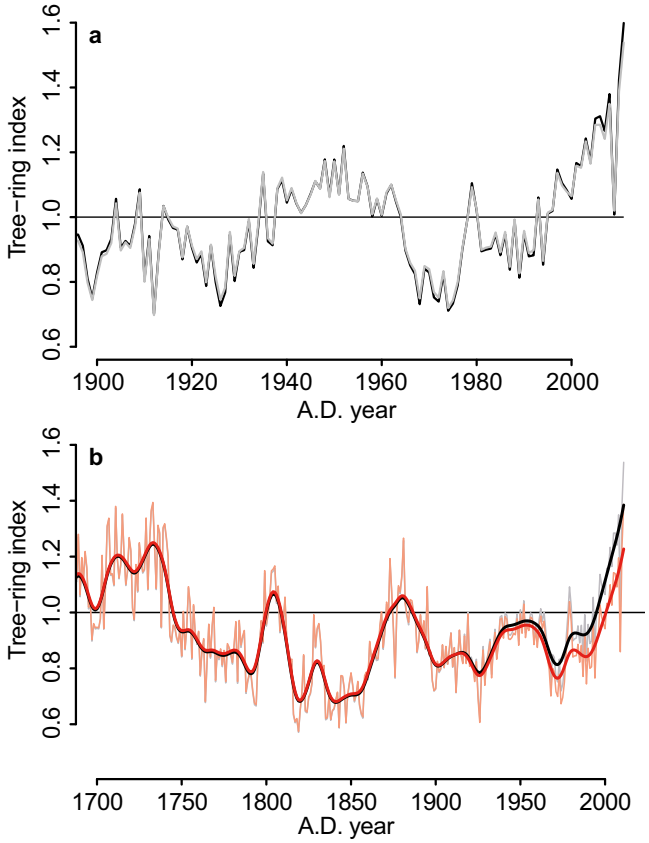

Fig. S2. Effects of removing the sampling height bias from the tree-ring series of living trees. (*A*) The Regional Curve Standardization (RCS) chronologies of L1 (site chosen as example) derived from only living trees over the last century. The local RCS chronology from uncorrected ring-width series of living trees is in black, while the same chronology from corrected series (i.e., the bias due to sampling height is removed from all ring-width series and the local growth curve of subfossil trees is used for standardization) is in gray. *A* shows that the correction of the sampling height bias is not affecting the RCS standardization results (i.e., sampling height bias can be removed and the local RCS chronology remains unchanged). The corrected ring-width series of living trees can subsequently be used together with those of subfossil samples to develop an unbiased RCS chronology (black line in *B*). The local RCS chronologies of L1 without correction of sampling height bias on the tree-ring series of living trees is shown for comparison (red line in *B*). In *B*, 20-y splines were used to smooth the values.

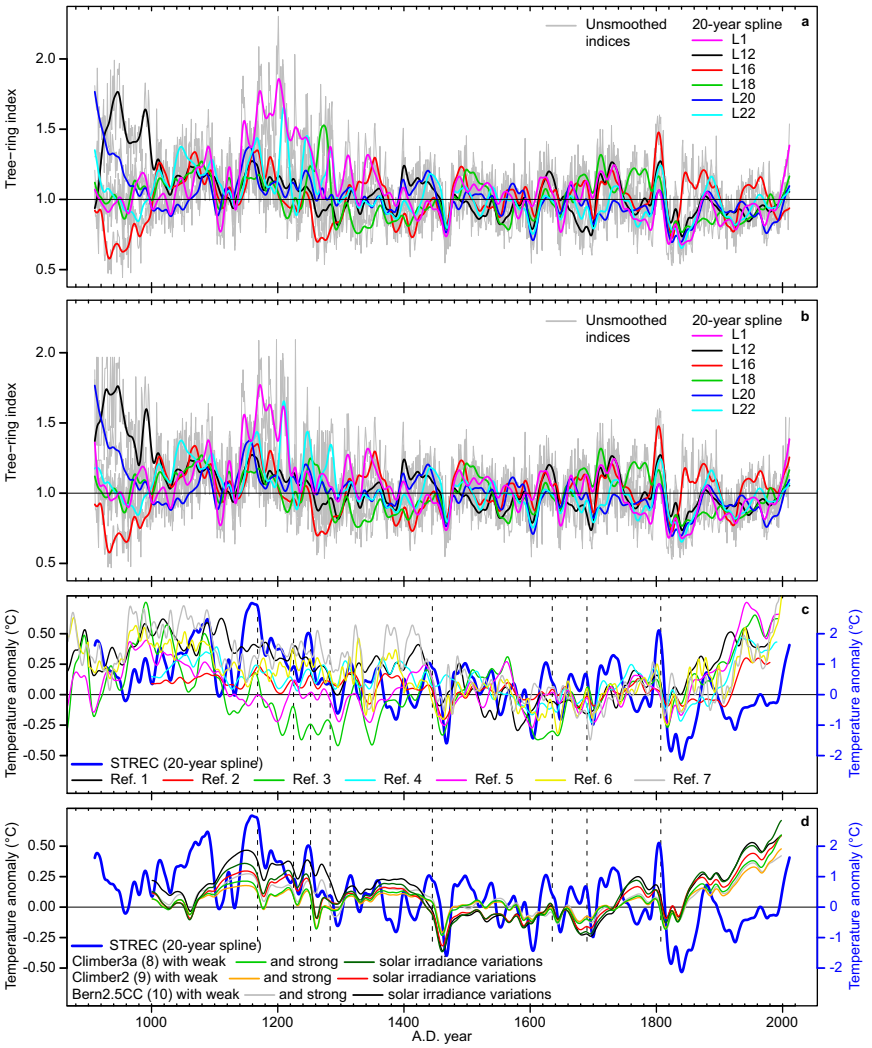

Fig. S3. The network of millennial-long tree-ring chronologies and comparison between STREC and other Northern Hemisphere records. (*A* and *B*) The six local RCS chronologies (one per lake and composed of living and subfossil trees) over the 1,102 y retained for STREC before (*A*) and after (*B*) the reconstruction of the nonrobust time intervals (i.e., intervals for each local chronology where the Rbar statistic calculated over the 31-y moving windows is lower or equal to zero or noncomputable because of low replication) using the analog method. (*C* and *D*) The comparison between STREC and seven Northern Hemisphere temperature reconstructions [refs. 1–7 (*C*)] and six Northern Hemisphere temperature simulations [three models, refs. 8–10, running twice with weak and strong solar irradiance variations and smoothed as plotted in figure 6.14 in ref. 11 (*D*)]. All records in *C* and *D* are expressed as anomalies from their 1500–1899 means. STREC has a larger variability than all other records due to its regional domain, so it is scaled on the *y* axis to improve the comparison (see blue labels). Vertical dashed lines highlight the beginning of synchronous cooling episodes in most records.

1. Moberg A, et al. (2005) Highly variable Northern Hemisphere temperatures reconstructed from low- and high-resolution proxy data. *Nature* 433(7026):613–617.
2. Mann ME, Bradley RS, Hughes MK (1999) Northern Hemisphere temperatures during the past millennium: Inferences, uncertainties, and limitations. *Geophys Res Lett* 26(6):759–762.
3. Cook ER, Esper J, D'Arrigo RD (2004) Extra-tropical Northern Hemisphere land temperature variability over the past 1000 years. *Quat Sci Rev* 23(20-22):2063–2074.
4. Jones PD, Briffa KR, Barnett TP, Tett SFB (1998) High-resolution palaeoclimatic records for the last millennium: Interpretation, integration and comparison with General Circulation Model control-run temperatures. *Holocene* 8(4):455–471.
5. D'Arrigo R, Wilson R, Jacoby G (2006) On the long-term context for late twentieth century warming. *J Geophys Res* 111(D3):D03103, 10.1029/2005JD006352.
6. Mann ME, et al. (2009) Global signatures and dynamical origins of the little ice age and medieval climate anomaly. *Science* 326(5957):1256–1260.
7. Mann ME, et al. (2008) Proxy-based reconstructions of hemispheric and global surface temperature variations over the past two millennia. *Proc Natl Acad Sci USA* 105(36): 13252–13257.
8. Montoya M, et al. (2005) The earth system model of intermediate complexity CLIMBER-3α. Part I: Description and performance for present-day conditions. *Clim Dyn* 25(2-3):237–263.
9. Petoukhov V, et al. (2000) CLIMBER-2: A climate system model of intermediate complexity. Part I: Model description and performance for present climate. *Clim Dyn* 16(1):1–17.
10. Plattner GK, Joos F, Stocker TF, Marchal O (2001) Feedback mechanisms and sensitivities of ocean carbon uptake under global warming. *Tellus B Chem Phys Meteorol* 53(5):564–592.
11. Jansen E, et al. (2007) Palaeoclimate. *Climate Change 2007: The Physical Science Basis. Contribution of Working Group I to the Fourth Assessment Report of the Intergovernmental Panel on Climate Change*, eds Solomon S, et al. (Cambridge Univ Press, Cambridge, UK), pp 433–497.

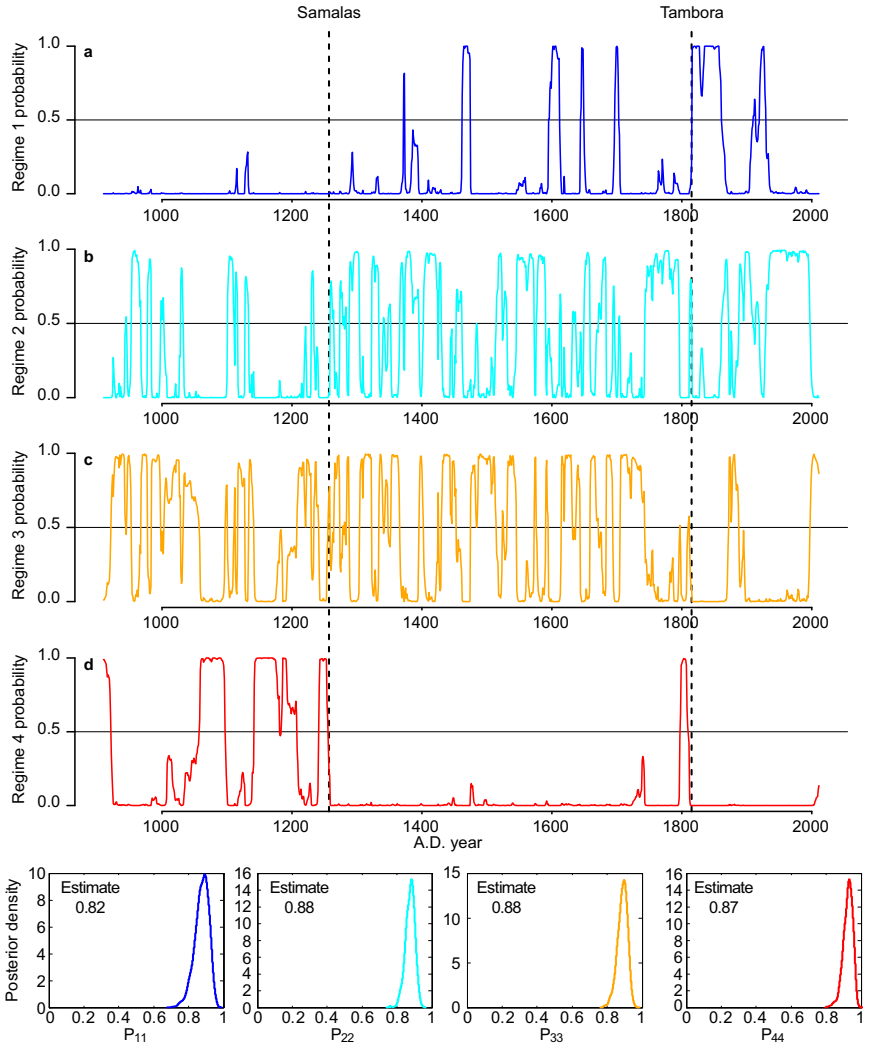

Fig. S4. Regime likelihood. Probability of STREC reconstructed temperature values to belong to any given regime of the four-component Bayesian hidden Markov model with normal distributions. (*Upper*) Regimes are ordered from the coldest to the warmest (*A*–*D*). (*Lower*) The posterior probability density functions of the transition probability p_{kk} of each regime. Regimes are ordered from the coldest (*Left*) to the warmest (*Right*).

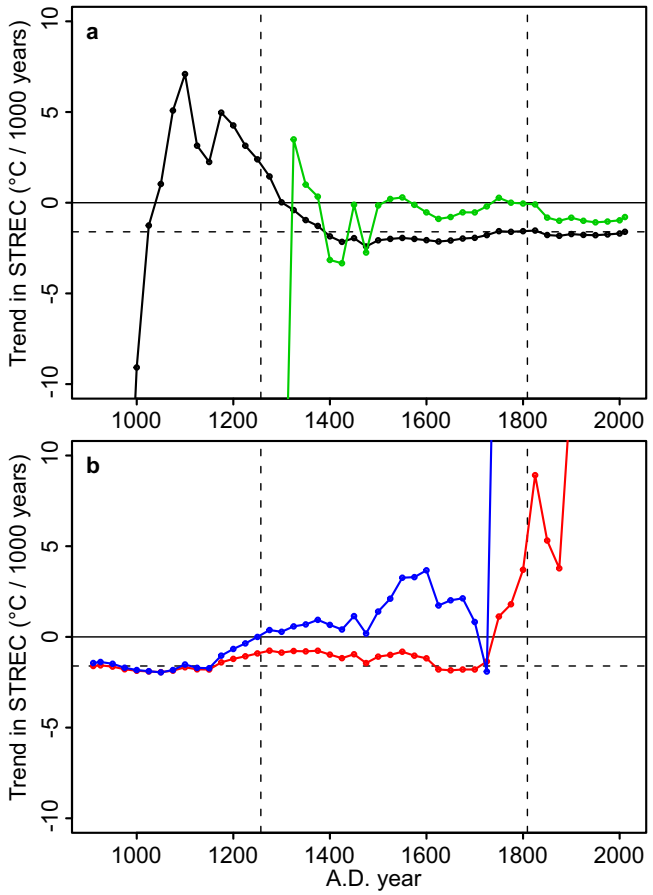

Fig. S5. Trends in STREC. In *A*, linear regression coefficients are obtained considering time periods starting from A.D. 910 (black) or A.D. 1257 (green) and increased by successive 25-y time steps (e.g., 910–950 with dot in 950, 910–975 with dot in 975...). In *B*, linear regression coefficients are obtained considering time periods starting from A.D. 2011 (red) or A.D. 1809 (blue) and lengthened backward by 25-y time steps (e.g., 1975–2011 with dot in 1975, 1950–2011 with dot in 1950...). The vertical dashed lines show the dates of the A.D. 1257 Samalas and A.D. 1809 (the event preceding the Tambora) eruptions, while the horizontal dashed line shows the trend over the entire time period covered by STREC (A.D. 910–2011; −1.6 °C per 1,000 y).

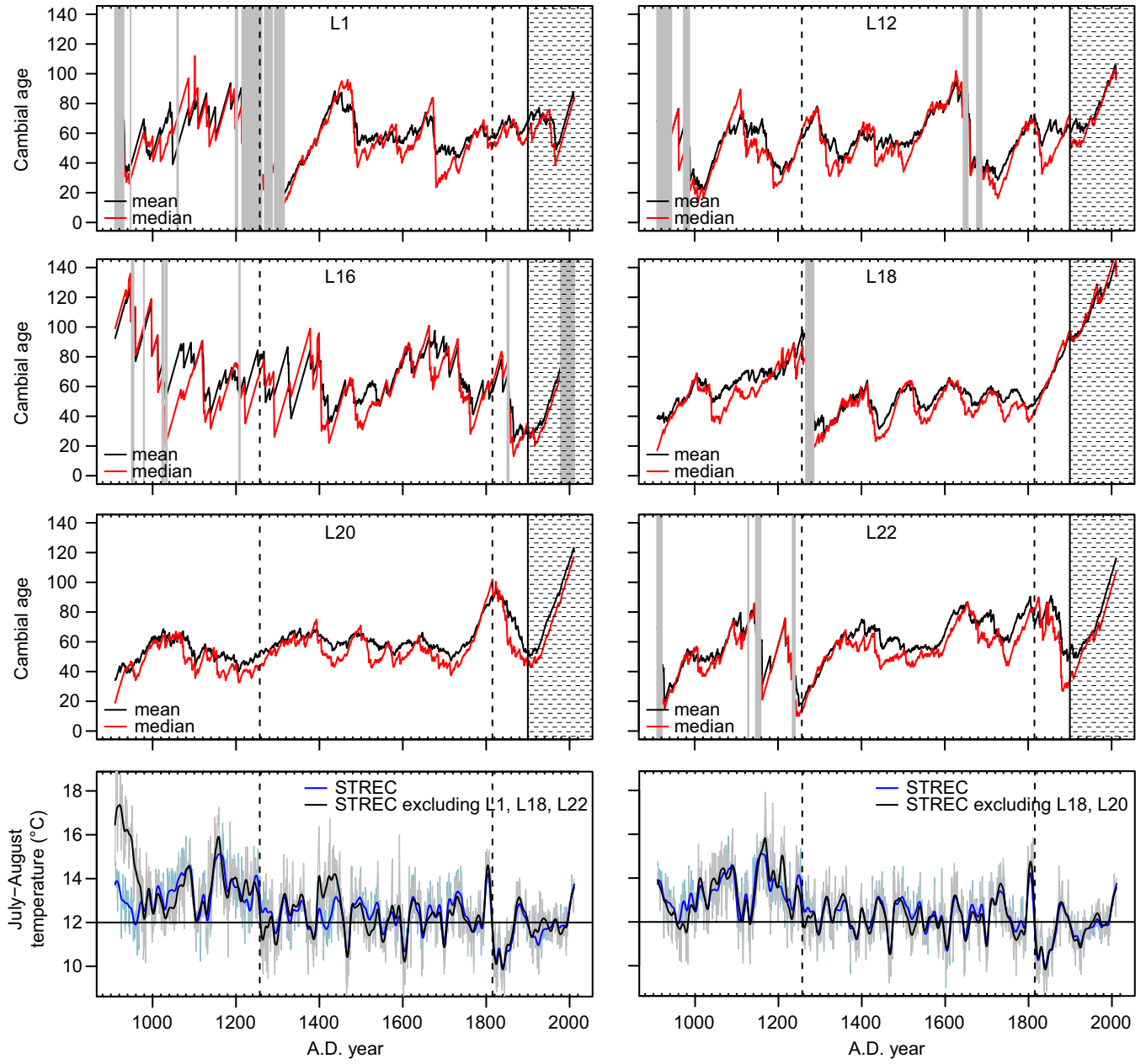

Fig. S6. (*Upper*) Time course of the mean and median cambial age for each local chronology (L1, L12, L16, L18, L20, and L22). Gray shadows show the time periods discarded for each chronology and reconstructed with the analog method. The dashed areas after A.D. 1900 show the time periods strongly influenced by living trees. The corrections applied on the ring-width series of living trees reduce possible biases in the RCS chronologies during these periods. The vertical dashed lines show the A.D. 1257 Samalas and A.D. 1815 Tambora eruptions. We tested if the most important regime shifts in STREC (i.e., post-A.D. 1257 and post-A.D. 1815) are artifacts due to local disturbances (mostly wildfires; see ref. 1) that changed the sample age structure through time in our chronologies [see *Lower* (July–August temperature)]. First, we compared STREC with an alternative reconstruction obtained by excluding those sites with unstable mean cambial age around A.D. 1257 (i.e., L1, L18, and L22). Second, we did the same exercise, but we excluded those sites with unstable mean cambial age around A.D. 1815 (i.e., L18 and L20). Smoothed values are 20-y splines. These alternative reconstructions show similar or even larger shifts at A.D. 1257 and A.D. 1815 compared with STREC suggesting that the regime shifts in STREC are robust.

1. Gennaretti F, Arseneault D, Bégin Y (2014) Millennial stocks and fluxes of large woody debris in lakes of the North American taiga. *J Ecol* 102(2):367–380.

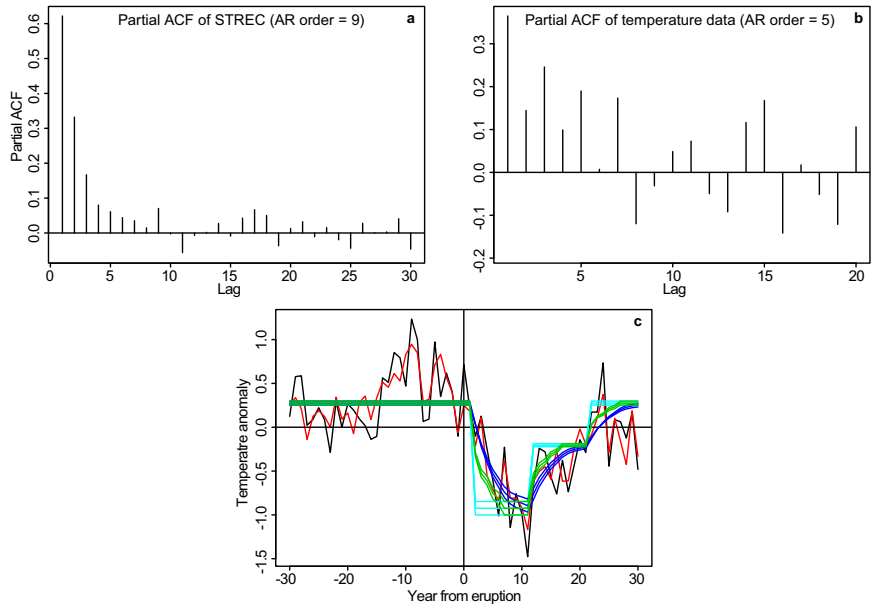

Fig. S7. Effect of autocorrelation on temperature anomalies after volcanic eruptions. (*A* and *B*) The estimates of the partial autocorrelation functions (partial ACF) fitted to STREC (*A*) and fitted to the July–August temperature data over the study area (*B*; 15 cells of the CRU TS3.20 dataset). The orders of the autoregressive model (AR order) selected by the Akaike Information Criterion are 9 and 5 for STREC and the temperature data, respectively. (*C*) The real mean (red) and median (black) responses of STREC to the 10 strongest volcanic eruptions of the last 1,100 y deduced by ref. 2, along with simulated temperature data (green) and simulated STREC (dark blue) after applying three different climate inputs (light blue) chosen to reduce the mean squared error between observed (red) and simulated (dark blue) STREC. Simulated temperature data were obtained with the formula $SimT_i = (\sum_{k=0}^{n} Input_{(i-k)} AC_k)/(\sum_{k=0}^{n} AC_k)$, where $SimT_i$ is the simulated temperature in the year *i*, *n* is the order of the autoregressive model fitted to the July–August temperature data over the study area, *k* is the lag of the partial autocorrelation function, $Input_{(i-k)}$ is the climate input in the year $(i-k)$, and AC_k is the estimate of lag *k* for the partial autocorrelation function fitted to the July–August temperature data over the study area (note that $AC_o = 1$). Here, we chose a two-step climate input composed of a constant reduction over 10 y starting from year 2 from eruptions (constant values were −1.1 °C, −1.2 °C, and −1.3 °C) followed by another constant reduction over 10 y (40% of the first reduction). Once the simulated temperatures were obtained, simulated STREC data were obtained with the formula $SimSTREC_i = (\sum_{k=0}^{n\_STREC} SimT_{(i-k)} AC\_STREC_k)/(\sum_{k=0}^{n\_STREC} AC\_STREC_k)$. The effect of autocorrelation of tree-ring data on STREC can be considered as the difference between the simulated temperatures (green) and the simulated STREC (dark blue).

Table S1. Summary of the cross-calibration verification results for the reconstruction of July–August temperatures using two different reconstruction methods

Statistics	Calibration over 1905–1957 (STREC/PLS-R)	Calibration over 1958–2011 (STREC/PLS-R)	Calibration over 1905–2011 (STREC/PLS-R)
Mean temperature of the 1905–2011 period, °C ± SD	11.9 ± 0.8/11.7 ± 0.5	11.8 ± 1.0/11.7 ± 0.8	11.9 ± 0.8/11.9 ± 0.7
Correlation over verification period	0.55/0.51	0.50/0.40	
Correlation over calibration period	0.44/0.53	0.55/0.68	
Correlation over total period	0.60/0.60	0.61/0.65	0.61/0.68
RMSE over verification period, °C	0.88/0.93	0.81/0.79	
RMSE over calibration period, °C	0.77/0.66	0.92/0.77	
RMSE over total period, °C	0.83/0.81	0.87/0.78	0.81/0.73
Significance of FDST over verification	1.00/1.00	0.76/0.99	
Significance of FDST over calibration	0.96/0.96	0.99/1.00	
Significance of FDST over total	1.00/1.00	0.98/1.00	1.00/1.00
RE	0.52/0.47	0.44/0.46	0.34/0.46*
CE	0.28/0.19	−0.07/-0.02	
RE on smoothed datasets (20-y spline)	0.85/0.73	0.90/0.70	0.83/0.90*
CE on smoothed datasets (20-y spline)	0.66/0.40	0.58/-0.17	

Reconstruction methods: a linear scaling procedure as in STREC and a reconstruction based on a partial least squares regression (PLS-R). Fifteen cells of the CRU TS3.20 dataset (1) covering our sampling sites are used as climate reference. FDST, first difference sign test (2); RE, reduction of error (3); CE, coefficient of efficiency (4).

*Computed over the total period and using the corresponding mean temperature as a reference.

1. Mitchell TD, Jones PD (2005) An improved method of constructing a database of monthly climate observations and associated high-resolution grids. *Int J Climatol* 25(6):693–712.
2. Cook ER, Kairiukstis LA (1990) *Methods of Dendrochronology: Applications in the Environmental Sciences* (Kluwer, Dordrecht, The Netherlands).
3. Fritts HC (1976) *Tree Rings and Climate* (Academic, London).
4. Briffa KR, Jones PD, Pilcher JR, Hughes MK (1988) Reconstructing summer temperatures in northern Fennoscandinavia back to AD 1700 using tree-ring data from Scots pine. *Arct Alp Res* 20(4):385–394.

Table S2. Results of the Wilcoxon rank–sum test (one-tailed)

Year of sulfate peak	Sulfate aerosol, Tg	10 or 20 y preevent mean (A), °C	10 or 20 y postevent mean (B), °C	B − A, °C	*P* value
10 strongest volcanic eruptions					
1167*	52.11	14.89	14.07	−0.83	0.02
1227*	67.52	13.06	13.18	0.12	0.54
1258*	257.91	13.70	12.43	−1.26	0.00
1275*	63.72	12.69	12.16	−0.53	0.06
1284*	54.70	12.47	11.90	−0.57	0.03
1452*	137.50	13.03	11.32	−1.71	0.00
1600*	56.59	11.97	11.44	−0.52	0.09
1783*	92.96	11.77	12.61	0.84	0.98
1809*	53.74	13.11	11.06	−2.05	0.00
1815*	109.72	13.55	10.58	−2.98	0.00
Composite*	NA	0.03†	−0.03†	−0.06†	0.00
10 next strongest volcanic eruptions					
1001‡	21.01	12.93	13.07	0.15	0.60
1176‡	45.76	14.84	13.49	−1.35	0.02
1341‡	31.14	12.46	12.46	0.00	0.43
1459‡	21.92	12.56	10.80	−1.76	0.00
1584‡	24.23	12.32	12.47	0.15	0.63
1641‡	51.59	12.47	11.37	−1.09	0.02
1693‡	27.10	12.85	11.07	−1.78	0.00
1719‡	31.48	12.99	13.08	0.09	0.76
1835‡	40.16	10.91	9.90	−1.01	0.01
1883‡	21.86	12.92	12.35	−0.57	0.02
Composite‡	NA	0.02†	−0.03†	−0.05†	0.00

The test was used to verify if the 20 or 10 postevent summers inferred by STREC were significantly colder than the preceding ones for each of the 10 strongest and each of the 10 next strongest volcanic eruptions of the last millennium (deduced by ref. 2), respectively. Composite, the average result of 10 eruptions as obtained by the SEA.

*Twenty years before and after the volcanic eruption are considered.

†Dimensionless normalized units.

‡Ten years before and after the volcanic eruption are considered.

Table S3. Extreme decades and temperature increases reconstructed by STREC

10 warmest decades			10 coldest decades			10 strongest temperature increases on a 30-y period		
Rank	Decade	Anomaly relative to 2002–2011, °C	Rank	Decade	Anomaly relative to 2002–2011, °C	Rank	Period	Increase, °C/10 y ± SE
1/90	1161–1170	1.80	1/90	1835–1844	−3.58	1/26	1128–1157	1.48 ± 0.20
2/90	1151–1160	1.68	2/90	1818–1827	−3.21	2/26	1600–1629	1.25 ± 0.21
3/90	1086–1095	1.19	3/90	1465–1474	−2.94	3/26	1462–1491	1.15 ± 0.23
4/90	1072–1081	1.00	4/90	1848–1857	−2.76	4/26	1778–1807	1.06 ± 0.20
5/90	1141–1150	0.89	5/90	1602–1611	−2.69	5/26	1852–1881	1.06 ± 0.15
6/90	1798–1807	0.87	6/90	1920–1929	−2.52	6/26	1697–1726	0.84 ± 0.20
7/90	1061–1070	0.87	7/90	1695–1704	−2.41	7/26	1293–1322	0.83 ± 0.15
8/90	1243–1252	0.83	8/90	1384–1393	−2.17	**8/26**	**1982–2011**	**0.78 ± 0.11**
9/90	1184–1193	0.73	9/90	1905–1914	−2.14	9/26	1414–1443	0.74 ± 0.15
10/90	910–919	0.61	10/90	1644–1653	−2.12	10/26	1229–1258	0.69 ± 0.20
19/90	**2002–2011**	**0.00**	**78/90**	**2002–2011**	**0.00**			

Overlapping decades or periods are excluded from the analysis. Intervals ending in 2011 are in bold.

Other Supporting Information Files

Dataset S1 (XLSX)